

# Convective invigoration traced to warm-rain microphysics

Xin Rong Chua<sup>1</sup> and Yi Ming<sup>2</sup>

<sup>1</sup>Centre for Climate Research Singapore

<sup>2</sup>Geophysical Fluid Dynamics Laboratory

November 24, 2022

## Abstract

Aerosols are postulated to alter moist convection by increasing cloud droplet number concentration (Nd). Cloud-resolving model simulations of radiative-convective equilibrium show that higher Nd leads to stronger convective mass flux, seemingly in line with a hypothesis that links the convective invigoration to delayed rain formation allowing more cloud liquid condensate to be frozen. Yet, the invigoration is also present in an alternative model configuration with warm-rain microphysics only, suggesting that ice microphysics is not central to the phenomenon. The key dynamical mechanism lies in the different vertical distributions of the increases in water vapor condensation and in cloud liquid re-evaporation, causing a dipole pattern favoring convection. This is further supported by a pair of mechanism-denial experiments in which an imposed weakening of cloud liquid re-evaporation tends to mute invigoration.

1                   **Convective invigoration traced to warm-rain**  
2                   **microphysics**

3                   **Xin Rong Chua<sup>1\*</sup>, Yi Ming<sup>1,2</sup>**

4                   <sup>1</sup>Program in Atmospheric and Oceanic Sciences, Princeton University, Princeton, New Jersey, USA

5                   <sup>2</sup>Geophysical Fluid Dynamics Laboratory/NOAA, Princeton, New Jersey, USA

6                   **Key Points:**

- 7                   • Higher cloud droplet number concentration increases convective mass flux, even  
8                   in the absence of ice microphysics.
- 9                   • The convective invigoration coincides with higher tropospheric relative humidity  
10                  and re-evaporation efficiency.
- 11                  • The dynamical mechanism involves a vertical dipole (cooling-above-warming) pat-  
12                  tern.

---

\*Current affiliation: Centre for Climate Research Singapore, Singapore

Corresponding author: Yi Ming, [Yi.Ming@noaa.gov](mailto:Yi.Ming@noaa.gov)

**Abstract**

Aerosols are postulated to alter moist convection by increasing cloud droplet number concentration ( $N_d$ ). Cloud-resolving model simulations of radiative-convective equilibrium show that higher  $N_d$  leads to stronger convective mass flux, seemingly in line with a hypothesis that links the convective invigoration to delayed rain formation allowing more cloud liquid condensate to be frozen. Yet, the invigoration is also present in an alternative model configuration with warm-rain microphysics only, suggesting that ice microphysics is not central to the phenomenon. The key dynamical mechanism lies in the different vertical distributions of the increases in water vapor condensation and in cloud liquid re-evaporation, causing a dipole pattern favoring convection. This is further supported by a pair of mechanism-denial experiments in which an imposed weakening of cloud liquid re-evaporation tends to mute invigoration.

**Plain Language Summary**

Aerosols are thought to affect moist convection by increasing cloud droplet number concentration. According to a popular hypothesis, higher droplet number concentration would delay rain formation, allowing more cloud water to reach the freezing level. The additional latent heating from freezing is presumed to cause stronger convection. We test this hypothesis with a numerical model capable of simulating moist convection, and find that convective invigoration occurs even in the absence of ice processes. A detailed analysis suggests that the slowdown of rain formation increases cloud liquid re-evaporation. The resulting cooling is balanced primarily by stronger water vapor condensation. This creates a vertical cooling-above-warming dipole pattern favorable to convection.

**1 Introduction**

Aerosols, natural and anthropogenic alike, alter Earth's radiative budget by scattering and/or absorbing shortwave radiation, as well as by altering cloud albedo (Twomey, 1974) and lifetime (Albrecht, 1989). Both effects have important implications for moist convection and precipitation. This work focuses on the purely microphysical pathway through which aerosols affect deep convective clouds by increasing cloud droplet number concentration ( $N_d$ ). A commonly referenced mechanism (Rosenfeld et al., 2008; Williams

et al., 2002; Andreae et al., 2004) posits that higher  $N_d$  leads to smaller droplets, thus delaying rain formation. This effect tends to bring more cloud liquid water above the freezing level, and the additional latent heat release would invigorate convection.

Stevens and Feingold (2009) hypothesized that delayed precipitation formation would allow more liquid to reach the cloud-top region of a cumulus. The resulting re-evaporative cooling has an effect of destabilizing the atmospheric column, and thus promoting convection. It was also acknowledged that this cloud-dynamical effect might be mitigated by more efficient precipitation production in deep clouds. More broadly, the re-evaporation of cloud condensate, by influencing cold pool strength, can exert a strong control on subsequent convection (e.g. Tao et al., 2007; Morrison, 2012; Tao et al., 2012). A recent study by Fan et al. (2018) suggested that ultrafine aerosol particles (smaller than 50 nm) can be activated into cloud droplets in a clean environment owing to higher in-cloud supersaturation; the additional droplets in return facilitate condensation. It was argued that the resulting convective invigoration occurs via a warm-phase (liquid) microphysical pathway based on the relatively small increase in upper-level latent heating. In other words, one does not have to rely on ice microphysics to explain the convective adjustment to aerosols.

To further complicate the matter, there is no consensus among the existing case studies on how aerosols would strengthen or weaken convection (see Morrison (2012) for a case of weakening). It is not straightforward to make comparison across different case studies given that environmental factors such as wind shear (e.g. Fan et al., 2009) and cloud-radiative effects (e.g. Fan et al., 2015) can potentially alter the eventual convective response. In contrast, the setting of radiative-convective equilibrium (RCE) makes it possible to diagnose which processes are of leading-order importance to the simulated quasi-steady state in a simple framework. For example, van den Heever et al. (2011) found an increase in the frequency of updrafts in response to increased  $N_d$ . In a follow-up study focusing on deep convective clouds, Storer and van den Heever (2013) showed that the freezing of cloud liquid is not among the largest contributors to the overall latent heat budget, suggesting that at least in RCE, freezing might not be as important for understanding convective invigoration as initially thought. This study is conceived as a targeted mechanistic study of the role of liquid microphysics in determining aerosol effects on convection.

## 75 2 Methodology

76 The RCE simulations are performed with the Weather Research and Forecasting  
 77 (WRF) model (Wang & Sobel, 2011), a widely used cloud-resolving model (CRM). The  
 78 configuration is identical to that used in Chua et al. (2019) except for the treatment of  
 79 cloud microphysics (as detailed later). The model domain is doubly periodic and con-  
 80 tains  $96 \times 96$  gridpoints at a horizontal resolution of 2 km with fifty vertical levels. At-  
 81 mospheric radiative cooling is prescribed at  $-1.5 \text{ K day}^{-1}$  in the troposphere (defined as  
 82 temperature warmer than 207.5 K). Elsewhere temperature is relaxed to 200 K over 5  
 83 days following a Newtonian relaxation scheme. Prescribing radiative cooling eliminates  
 84 a major confounding factor common to this type of studies. Surface sensible and latent  
 85 heat fluxes are computed with an aerodynamic formulation at a constant near-surface  
 86 wind speed of  $5 \text{ m s}^{-1}$ . The surface temperature is set at 301 K. Subgrid diffusion is cal-  
 87 culated with the Smagorinsky and YSU schemes (Hong et al., 2006). Domain-average  
 88 winds are nudged to zero on a time scale of two hours.

89 The model uses the the double-moment Morrison cloud microphysics scheme (Morrison  
 90 et al., 2009). By tracking both mass mixing ratios and numbers of hydrometeors, a double-  
 91 moment scheme is deemed to be more suitable for simulating the microphysical effects  
 92 of aerosols on moist convection than a single-moment scheme of mixing ratios. The warm-  
 93 rain or liquid part of the scheme is described briefly here as it is important for under-  
 94 standing the results. Water vapor ( $q_v$ ) condenses into cloud liquid ( $q_l$ ) through satura-  
 95 tion adjustment. Note that  $q$  denotes mass mixing ratio. Re-evaporation of cloud liq-  
 96 uid occurs only under subsaturated conditions. Cloud liquid converts into rain ( $q_r$ ) through  
 97 either autoconversion or accretion; the rates are parameterized as  $1350q_l^{2.47}N_d^{-1.79}$  and  
 98  $67(q_lq_r)^{1.15}$ , respectively (Khairoutdinov & Kogan, 2000). Note that  $q_l$  and  $q_r$  are in  $\text{kg}$   
 99  $\text{kg}^{-1}$ ,  $N_d$  in  $\text{cm}^{-3}$  and the rates in  $\text{kg kg}^{-1} \text{ s}^{-1}$ . Autoconversion is the only microphys-  
 100 ical process that is controlled directly by  $N_d$ . Rain can re-evaporate back into water va-  
 101 por.

102 Three alternative configurations are created from simplifying the full model (re-  
 103 ferred to as FU). One can turn off the ice part of the Morrison scheme. In the result-  
 104 ing configuration (referred to as LI), the liquid microphysics operates at all temperatures.  
 105 The formulae used for computing the cloud liquid and rain re-evaporation rates are scaled

106 by a factor of 0.1 in the CE and RE configurations, respectively. This does not mean that  
 107 the actual rates would decrease by 10 times as other factors may also vary.

108 For each of the four model configurations (i.e. FU, LI, CE and RE), a pair of sim-  
 109 ulations are performed.  $N_d$  is set to  $100 \text{ cm}^{-3}$  in the control experiment, and  $1000 \text{ cm}^{-3}$   
 110 in the perturbation experiment. The former is denoted by the name of a configuration,  
 111 and the latter by adding an asterisk. For example, the control and perturbation exper-  
 112 iments performed with the full model are referred to as FU and FU\*, respectively.

113 A control experiment is initialized from a warm bubble, and is integrated for 240  
 114 model days. The output at Day 180 is used to initialize a corresponding 60-day pertur-  
 115 bation experiment. We analyze the last 20 days of hourly-mean outputs from each sim-  
 116 ulation. The noise level of a given variable is quantified using five consecutive, non-overlapping  
 117 20-day periods from an extended full model control simulation (namely FU).

### 118 **3 Results**

119 Some key characteristics of the control simulations and their changes in response  
 120 to higher  $N_d$  are depicted in Figure 1. The distributions of cloud liquid ( $q_l$ ) in the lower  
 121 and mid-troposphere are similar among all four configurations, with a distinct peak at  
 122 around 900 hPa (Figure 1a). As designed, high clouds are comprised of ice ( $q_i$ ) in FU,  
 123 and liquid in the other cases. Interestingly, the upper-tropospheric  $q_l$  in LI and CE is  
 124 comparable to  $q_i$  in FU, but much higher than  $q_l$  in RE. Higher  $N_d$  gives rise to an in-  
 125 crease in cloud condensate below 500 hPa in all cases (Figure 1b). CE is opposite to the  
 126 other three cases in showing a substantial increase in high cloud condensate.

127 In FU, rain ( $q_r$ ) is concentrated mostly below 500 hPa, while snow and graupel (col-  
 128 lectively referred to as snow,  $q_s$ ) dominates above. The three liquid microphysics con-  
 129 trol simulations exhibit almost identical vertical distributions of rain throughout the col-  
 130 umn, which are bottom-heavy with maxima at around 700 hPa (Figure 1c). Elevated  
 131  $N_d$  causes  $q_r$  to decrease in all cases below 600 hPa, and to increase in the three liquid  
 132 microphysics cases above, albeit to varying degrees (Figure 1d).  $q_s$  in FU increases as  
 133 well. Taken together, the increase in cloud liquid and the concurrent decrease in rain in  
 134 the lower troposphere are consistent with the microphysical nature of the perturbation,  
 135 i.e. higher  $N_d$  tending to suppress the conversion of cloud liquid to rain, while convec-  
 136 tive adjustment seems to play a prominent role in shaping the upper-tropospheric changes.

137 Convective mass flux ( $M_c$ ) is computed by summing the mass flux at gridpoints  
 138 where the total cloud condensate ( $q_c$ , or  $q_l + q_i$ ) is greater than  $0.005 \text{ g kg}^{-1}$  and ver-  
 139 tical velocity exceeds  $1 \text{ m s}^{-1}$  (Wang & Sobel, 2011). In much of the troposphere,  $M_c$   
 140 in FU is substantially (about 40%) stronger than in the liquid microphysics cases (Fig-  
 141 ure 1e). They also differ in vertical structures; FU has only one in the lower troposphere,  
 142 while the latter have two peaks, one in the lower troposphere and the other in the up-  
 143 per troposphere.  $M_c$  shows a substantial increase below 500 hPa due to higher  $N_d$ , which  
 144 amounts to  $\sim 30\%$  at 600 hPa (Figure 1f). The convective invigoration is accompanied  
 145 by a relatively small decrease in  $M_c$  in the upper troposphere in FU\* and LI\*. The mag-  
 146 nitude of the enhancement of  $M_c$  is fully captured in LI, suggesting that ice microphysics  
 147 is not essential for explaining the convective invigoration, contrary to Rosenfeld et al.  
 148 (2008). Furthermore, the invigoration is muted in the configuration of CE, indicating  
 149 that cloud liquid re-evaporation may be a key process involved in the convective response.  
 150 In contrast, RE does not show any appreciable difference from LI, which hints at a sec-  
 151 ondary role played by rain re-evaporation. Note that none of the simulations examined  
 152 here shows any sign of self-aggregation.

153 Figure 1g shows the relative humidity ( $RH$ ) in the control cases. The vertical pro-  
 154 files take a C-shape, with minima at around 500 hPa. FU, however, has notably higher  
 155 mid-tropospheric  $RH$  ( $\sim 70\%$ ) than the liquid microphysics cases ( $\sim 40\%$ ), suggesting that  
 156 ice microphysics is crucial for moistening the mid-troposphere. A comparison of RE and  
 157 LI indicates that rain re-evaporation is also an important source of mid-tropospheric mois-  
 158 ture, while cloud liquid re-evaporation is not (CE versus LI). Across all cases,  $RH$  shows  
 159 a pronounced increase below 500 hPa owing to higher  $N_d$  (Figure 1h). With the excep-  
 160 tion of CE, they all experience lower  $RH$  in the upper troposphere.

161 The impression from Figures 1(f) and (h) that convective invigoration coincides  
 162 with mid-tropospheric moistening is formalized in Figure 2. The vertically averaged con-  
 163 vective mass flux ( $[M_c]$ ) in the various control and perturbation experiments is gener-  
 164 ally positively correlated with the column-average relative humidity ( $CRH$ ). The cor-  
 165 relation with the mid-tropospheric (400 to 600 hPa) relative humidity ( $MRH$ ) is even  
 166 stronger. This relationship holds not only for every pair of control and perturbation ex-  
 167 periments but also for all the control experiments. Although it is well established that  
 168 a moist mid-troposphere is conducive to convective development (e.g. in the context of  
 169 tropical cyclones), convective detrainment of cloud condensate is an important supplier

170 of mid-tropospheric moisture. These two mechanisms are not mutually exclusive, and  
 171 work in the same direction. This work does not attempt to address the relative roles of  
 172 these mechanisms, which would be difficult to separate in a clean way.

173 The need to better understand the controlling factors of  $RH$  prompts us to exam-  
 174 ine the moisture budget. The column-integrated source and sink terms, along with the  
 175 changes caused by increased  $N_d$ , are given in Table 1. To facilitate the discussion, they  
 176 are also illustrated in Figure 3 for the LI configuration. For water vapor, condensation  
 177 ( $C$ ) is balanced by surface evaporation ( $ES$ ), and re-evaporation of cloud condensate and  
 178 rain ( $EC$  and  $ER$ , respectively). The conversion from cloud liquid to rain is realized through  
 179 autoconversion ( $CR$ ) and accretion ( $AR$ ). Although autoconversion is almost negligi-  
 180 ble in terms of domain average (consistent with other cloud-resolving simulations (e.g.  
 181 Heikenfeld et al., 2019)), it is the only process through which rain formation can occur  
 182 spontaneously – a necessary condition for accretion that involves both cloud liquid and  
 183 rain simultaneously. In this sense, it is conceivable that a perturbation to the former,  
 184 however small in magnitude, may still affect the latter. Rain is partitioned between re-  
 185 evaporation ( $ER$ ) and surface precipitation ( $P$ ).

186 The re-evaporation efficiency ( $\alpha$ ) is defined as the ratio of the total re-evaporation  
 187 ( $E$ , or the sum of  $EC$  and  $ER$ ) to  $C$  (Romps, 2014). Note that one definition of the widely  
 188 used quantity called precipitation efficiency is the ratio of surface precipitation ( $P$ ) to  
 189  $C$  (e.g. Langhans et al., 2015; Lutsko & Cronin, 2018). Thus,  $\alpha$  is one minus the pre-  
 190 cipitation efficiency. Dictated, to the zeroth order, by the free-tropospheric radiative cool-  
 191 ing rate, the domain-average  $ES$  or  $P$  is little changed regardless of the configurations  
 192 or perturbations. Both  $C$  and  $E$  are substantially lower in LI than in FU, but the frac-  
 193 tional decrease in  $E$  is greater than that in  $C$ . This results in a net decrease in  $\alpha$ . As  
 194 expected, weakening the re-evaporation processes tends to lower  $\alpha$ , albeit to different ex-  
 195 tents.  $\alpha$  is more sensitive to the perturbation to rain re-evaporation than that to cloud  
 196 liquid re-evaporation, implying that  $EC$  is limited more strongly by the availability of  
 197 cloud liquid as opposed to the prescribed rate constant.

198 Higher  $N_d$  leads to a slowdown in accretion by modulating autoconversion. This  
 199 is consistent with higher  $q_l$  and lower  $q_r$  (Figures 1b and d). As explained before, since  
 200  $P$  is somewhat fixed, and  $\delta CR$  is small,  $\delta AR$  must be approximately equal to  $\delta ER$  (with  
 201  $\delta$  denoting changes). This explains why rain re-evaporation decreases. Higher  $q_l$  is con-

202 sistent with stronger  $EC$  as they are directly linked. Since  $P$  is approximately unchanged,  
 203 it follows that  $\delta C \simeq \delta ER + \delta EC$ . This relation, however, does not help constrain the  
 204 sign of  $\delta C$  as  $\delta ER$  and  $\delta EC$  are of opposite signs. It seems plausible to assume that  $C$   
 205 and  $EC$  would vary in the same direction as they are the dominant sink and source terms  
 206 in the cloud liquid budget, an issue to which we will return later.

207 Invoking  $\delta C \simeq \delta E$ , one can write  $\delta\alpha$  approximately as  $(1 - \alpha)\delta C / (C + \delta C)$ . If it  
 208 is assumed that  $\delta C \ll C$ , the expression can be further simplified to  $\delta\alpha \simeq (1 - \alpha)\delta C / C$ .  
 209 This simple theory is found to be in good agreement with the simulated  $\delta\alpha$  (Table 1).  
 210 Thus, the increase in  $\alpha$  can be thought of as a manifestation of stronger condensation.

211 Across all the cases,  $\alpha$  is strongly correlated with column relative humidity ( $CRH$ )  
 212 (Figure 2c), and to a lesser extent, with mid-tropospheric relative humidity ( $MRH$ ) (Fig-  
 213 ure 2d). This result is qualitatively consistent with an analytical model of tropospheric  
 214 relative humidity in RCE (Romps, 2014), in which cloud condensate re-evaporation is  
 215 treated as an important mechanism for moistening the environment. In particular,  $\alpha$  is  
 216 smaller than  $CRH$ , conforming to the constraint inferred from the analytical model. This  
 217 line of reasoning appears to suggest that the microphysical perturbation caused by higher  
 218  $N_d$  tends to increase the re-evaporation efficiency. The resulting tropospheric moisten-  
 219 ing creates a favorable environment for convection.

220 As appealing as the above explanation is, it does not yield insights into the dynam-  
 221 ics underlying the convective invigoration. The microphysical processes discussed above  
 222 can be divided into two categories depending on whether phase change is involved. The  
 223 latent heating from condensation ( $C$ ) and the latent cooling from rain and cloud con-  
 224 densation re-evaporation ( $ER$  and  $EC$ , respectively) play crucial roles in the energy bal-  
 225 ance, and have to be in equilibrium with other diabatic (e.g. radiative) and dynamical  
 226 terms (resolved and implicit). In contrast, accretion is not part of the energy balance.  
 227 Furthermore, the latent heating and cooling have distinct vertical structures as illustrated  
 228 in Figure 4. In all the control experiments, the condensational heating peaks much lower  
 229 ( $\sim 900$  hPa) than the re-evaporative cooling (600 to 700 hPa). Conceptually, the former  
 230 generates positive buoyancy for lifting an air parcel. As the parcel rises, it entrains drier/colder  
 231 environmental air and detrains cloud condensate, which then re-evaporates into the en-  
 232 vironment. Similar to condensation, the total heating is bottom-heavy, but with a dis-  
 233 tinct local minimum owing to re-evaporation.

234 Both condensation and cloud liquid re-evaporation are stronger in the perturbed  
 235 energy balance, with a secondary weakening of rain re-evaporation. Although the com-  
 236 bined effect is integrated vertically to near zero, it is characteristic of a dipole (cooling  
 237 above warming) structure as  $\delta C$  is more bottom-heavy than  $\delta EC$ . The positive buoy-  
 238 ancy resulting from this pattern is consistent with the enhancement of  $M_c$  (Figure 1f).  
 239 Given that the initial perturbation is applied through modifying cloud liquid, one may  
 240 speculate that it is the stronger re-evaporative cooling that destabilizes the lower tro-  
 241 posphere and promotes stronger convection (condensation). This explains why conden-  
 242 sation and cloud liquid re-evaporation vary in the same direction, and constitutes a dy-  
 243 namical mechanism of the microphysically induced convective adjustment.

#### 244 4 Discussion and Conclusions

245 As an anchor point of this work, the re-evaporation efficiency ( $\alpha$ ) is an emergent  
 246 property of the RCE simulations, and is closely associated with tropospheric relative hu-  
 247 midity and convective mass fluxes across a wide range of model configurations and per-  
 248 turbations. It has been shown that the increase in  $\alpha$  due to higher  $N_d$  can be linked to  
 249 stronger condensation by invoking the simple theory ( $\delta\alpha \simeq (1 - \alpha)\delta C/C$ ), which can  
 250 also be used to explain, at least qualitatively, the large difference in  $\alpha$  among the four  
 251 control experiments (from 0.368 in RE to 0.664 in FU). Although it is clear from our re-  
 252 sults that the treatment of cloud microphysics has a direct bearing on  $\alpha$ , convective dy-  
 253 namics also plays an essential role, as evidenced by the destabilizing effect of cloud liq-  
 254 uid re-evaporation. In light of its importance for understanding tropospheric relative hu-  
 255 midity (Romps, 2014), convectively coupled tropical variations and general circulation  
 256 (Emanuel, 2019) and climate sensitivity (Zhao et al., 2016), the potential use of  $\alpha$  for  
 257 comparing a variety of model simulations (limited-domain and global CRMs, and coarse-  
 258 resolution global climate models or GCMs) and observations (Noone, 2012) should be  
 259 explored.

260 A contemporaneous study by Abbott and Cronin (2020) offers a way to examine  
 261 the robustness of our results to the choice of model configurations and experimental de-  
 262 signs. Both studies find that an increase in  $N_d$  gives rise to higher mid-tropospheric re-  
 263 lative humidity and convective invigoration in RCE simulations, even in the absence of  
 264 ice microphysics. While this work centers over convective invigoration (manifested as stronger

265 convective mass flux) in RCE, Abbott and Cronin (2020) focuses on changes in high-percentile  
266 vertical velocities under the assumption of weak temperature gradient balance.

267 Ice microphysical processes are often thought to play a key role in enhancing con-  
268 vection under polluted conditions. In the setting of RCE with prescribed radiative cool-  
269 ing, we demonstrate that an increase in cloud droplet number concentration can cause  
270 stronger convective mass flux even in the absence of ice microphysics. Subsequent sen-  
271 sitivity tests of liquid microphysical processes indicate that cloud liquid re-evaporation  
272 plays a more important role in driving the convective invigoration than rain re-evaporation.  
273 A process-level analysis reveals that higher cloud droplet number concentration slows  
274 down the conversion of cloud liquid to rain, giving rise to an increase in cloud liquid re-  
275 evaporation and a decrease in rain re-evaporation, with the former outweighing the lat-  
276 ter. The net increase in the total re-evaporation is balanced by stronger condensation.  
277 The dipole pattern of re-evaporative cooling above condensational heating is consistent  
278 with the enhancement of convective mass flux.

## 279 Acknowledgments

280 Data and scripts used in this paper will be archived at `ftp://data1.gfdl.noaa`  
281 `.gov/users/Xin.Rong.Chua/WRF_heat/WRF`. We thank Tristan Abbott, Tim Cronin, Nadir  
282 Jeevanjee, Hugh Morrison, Ming Zhao, Hailey Shin, Usama Anber and Spencer Clark  
283 for helpful discussions, Shuguang Wang for providing the source code for the WRF model  
284 used in this study, and the developers of the “aospy” package. XRC was funded by the  
285 Cooperative Institute for Modeling the Earth System (CIMES) at Princeton University  
286 and the Singapore National Research Foundation.

## 287 References

- 288 Abbott, T. H., & Cronin, T. W. (2020). A humidity-entrainment mechanism for mi-  
289 crophysical invigoration of convection. *arXiv*.
- 290 Albrecht, B. A. (1989, Sep 15). Aerosols, cloud microphysics, and fractional cloudi-  
291 ness. *Science*, *245*(4923), 1227.
- 292 Andreae, M. O., Rosenfeld, D., Artaxo, P., Costa, A. A., Frank, G. P., Longo,  
293 K. M., & Silva-Dias, M. A. F. (2004). Smoking rain clouds over the Ama-  
294 zon. *Science*, *303*(5662), 1337–1342.

- 295 Chua, X. R., Ming, Y., & Jeevanjee, N. (2019). Investigating the fast response of  
296 precipitation intensity and boundary layer temperature to atmospheric heating  
297 using a cloud-resolving model. *Geophysical Research Letters*, *46*(15), 9183-  
298 9192. Retrieved from [https://agupubs.onlinelibrary.wiley.com/doi/abs/  
299 10.1029/2019GL082408](https://agupubs.onlinelibrary.wiley.com/doi/abs/10.1029/2019GL082408) doi: 10.1029/2019GL082408
- 300 Emanuel, K. (2019). Inferences from simple models of slow, convectively coupled  
301 processes. *Journal of the Atmospheric Sciences*(2019). doi: 10.1175/JAS-D-18  
302 -0090.1
- 303 Fan, J., Rosenfeld, D., Yang, Y., Zhao, C., Leung, L. R., & Li, Z. (2015). Sub-  
304 substantial contribution of anthropogenic air pollution to catastrophic floods in  
305 Southwest China. *Geophysical Research Letters*, *42*(14), 6066–6075.
- 306 Fan, J., Rosenfeld, D., Zhang, Y., Giangrande, S. E., Li, Z., Machado, L. A., . . .  
307 others (2018). Substantial convection and precipitation enhancements by  
308 ultrafine aerosol particles. *Science*, *359*(6374), 411–418.
- 309 Fan, J., Yuan, T., Comstock, J. M., Ghan, S., Khain, A., Leung, L. R., . . . Ovchin-  
310 nikov, M. (2009). Dominant role by vertical wind shear in regulating aerosol  
311 effects on deep convective clouds. *Journal of Geophysical Research: Atmo-  
312 spheres*, *114*(D22).
- 313 Heikenfeld, M., White, B., Labbouz, L., & Stier, P. (2019). Aerosol effects on deep  
314 convection: the propagation of aerosol perturbations through convective cloud  
315 microphysics. *Atmospheric Chemistry and Physics*, *19*(4), 2601–2627.
- 316 Hong, S.-Y., Noh, Y., & Dudhia, J. (2006). A new vertical diffusion package with an  
317 explicit treatment of entrainment processes. *Monthly Weather Review*, *134*(9),  
318 2318–2341.
- 319 Khairoutdinov, M., & Kogan, Y. (2000). A new cloud physics parameterization in  
320 a large-eddy simulation model of marine stratocumulus. *Monthly Weather Re-  
321 view*, *128*(1), 229–243.
- 322 Langhans, W., Yeo, K., & Romps, D. M. (2015). Lagrangian investigation of the  
323 precipitation efficiency of convective clouds. *Journal of the Atmospheric Sci-  
324 ences*, *72*(3), 1045–1062.
- 325 Lutsko, N. J., & Cronin, T. W. (2018). Increase in precipitation efficiency with sur-  
326 face warming in radiative-convective equilibrium. *Journal of Advances in Mod-  
327 eling Earth Systems*.

- 328 Morrison, H. (2012). On the robustness of aerosol effects on an idealized supercell  
329 storm simulated with a cloud system-resolving model. *Atmospheric Chemistry  
330 and Physics*, *12*(16), 7689–7705.
- 331 Morrison, H., Thompson, G., & Tatarskii, V. (2009). Impact of cloud microphysics  
332 on the development of trailing stratiform precipitation in a simulated squall  
333 line: Comparison of one-and two-moment schemes. *Monthly Weather Review*,  
334 *137*(3), 991–1007.
- 335 Noone, D. (2012). Pairing measurements of the water vapor isotope ratio with  
336 humidity to deduce atmospheric moistening and dehydration in the tropical  
337 midtroposphere. *Journal of Climate*, *25*(13), 4476–4494.
- 338 Romps, D. M. (2014). An analytical model for tropical relative humidity. *Journal of  
339 Climate*, *27*(19), 7432–7449.
- 340 Rosenfeld, D., Lohmann, U., Raga, G. B., O’Dowd, C. D., Kulmala, M., Fuzzi, S.,  
341 ... Andreae, M. O. (2008). Flood or drought: how do aerosols affect precipita-  
342 tion? *Science*, *321*(5894), 1309–1313.
- 343 Stevens, B., & Feingold, G. (2009). Untangling aerosol effects on clouds and precipi-  
344 tation in a buffered system. *Nature*, *461*(7264), 607.
- 345 Storer, R. L., & van den Heever, S. C. (2013). Microphysical processes evident in  
346 aerosol forcing of tropical deep convective clouds. *Journal of the Atmospheric  
347 Sciences*, *70*(2), 430–446.
- 348 Tao, W.-K., Chen, J.-P., Li, Z., Wang, C., & Zhang, C. (2012). Impact of aerosols  
349 on convective clouds and precipitation. *Reviews of Geophysics*, *50*(2).
- 350 Tao, W.-K., Li, X., Khain, A., Matsui, T., Lang, S., & Simpson, J. (2007). Role  
351 of atmospheric aerosol concentration on deep convective precipitation: Cloud-  
352 resolving model simulations. *Journal of Geophysical Research: Atmospheres*,  
353 *112*(D24).
- 354 Twomey, S. (1974). Pollution and the planetary albedo. *Atmospheric Environment*,  
355 *8*(12), 1251–1256.
- 356 van den Heever, S. C., Stephens, G. L., & Wood, N. B. (2011). Aerosol indirect  
357 effects on tropical convection characteristics under conditions of radiative-  
358 convective equilibrium. *Journal of the Atmospheric Sciences*, *68*(4), 699–718.
- 359 Wang, S., & Sobel, A. H. (2011). Response of convection to relative sea surface tem-  
360 perature: Cloud-resolving simulations in two and three dimensions. *Journal of*

361 *Geophysical Research: Atmospheres*, 116(D11).

362 Williams, E., Rosenfeld, D., Madden, N., Gerlach, J., Gears, N., Atkinson, L., . . .  
363 others (2002). Contrasting convective regimes over the Amazon: Implica-  
364 tions for cloud electrification. *Journal of Geophysical Research: Atmospheres*,  
365 107(D20), LBA-50.

366 Zhao, M., Golaz, J.-C., Held, I. M., Ramaswamy, V., Lin, S.-J., Ming, Y., . . . others  
367 (2016). Uncertainty in model climate sensitivity traced to representations of  
368 cumulus precipitation microphysics. *Journal of Climate*, 29(2), 543-560.

**Table 1.** Domain-average column-integrated condensation ( $C$ ), total re-evaporation ( $E$ ), rain re-evaporation ( $ER$ ), cloud condensate re-evaporation ( $EC$ ), accretion ( $AR$ ), precipitation ( $P$ ) in different cases. Also included is the re-evaporation efficiency ( $\alpha$ ). The differences between the control and perturbation simulations (the latter minus the former) are in parentheses. Except for  $\alpha$  (unitless), all values are in  $\text{mm day}^{-1}$ . The last column ( $\widetilde{\delta\alpha}$ ) is based on a simple theory for  $\delta\alpha$ , i.e.  $(1 - \alpha)\delta C/C$ .

	$C$	$E$	$ER$	$EC$	$AR$	$P$	$\alpha$	$\widetilde{\delta\alpha}$
FU	13.7 (0.9)	9.1 (0.8)	3.7 (-0.7)	5.4 (1.5)	8.2 (-0.6)	4.5 (0.1)	0.664 (0.014)	0.022
LI	10.2 (1.1)	5.8 (1.0)	2.7 (-0.6)	3.1 (1.6)	7.1 (-0.5)	4.5 (0.1)	0.569(0.033)	0.046
RE	7.6 (1.3)	2.8 (1.3)	0.5 (-0.2)	2.3 (1.4)	5.2 (-0.1)	4.7 (0.1)	0.368 (0.092)	0.108
CE	9.1 (0.5)	4.7 (0.5)	2.7 (-0.6)	2.0 (1.1)	7.1 (-0.6)	4.4 (0.0)	0.505 (0.026)	0.027

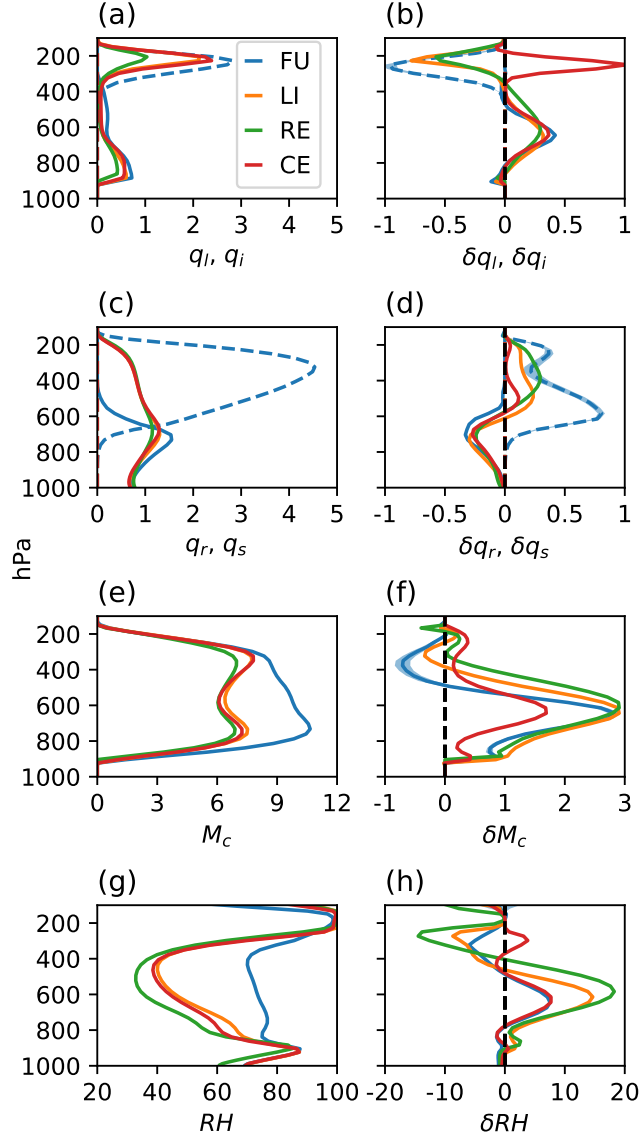


**Figure 1.** Vertical profiles of the domain-average (a)-(b) cloud liquid (solid,  $q_l$ ,  $10^{-5} \text{ kg}^{-1} \text{ kg}^{-1}$ ) or ice (dashed,  $q_i$ ,  $10^{-5} \text{ kg}^{-1} \text{ kg}^{-1}$ ) mixing ratio, (c)-(d) rain (solid,  $q_r$ ,  $10^{-5} \text{ kg}^{-1} \text{ kg}^{-1}$ ) or snow (dashed,  $q_s$ ,  $10^{-5} \text{ kg}^{-1} \text{ kg}^{-1}$ ) mixing ratio, (e)-(f) convective mass flux ( $M_c$ ,  $\text{g m}^{-2} \text{ s}^{-1}$ ) and (g)-(h) relative humidity ( $RH$ , %). The control experiments are in the left column, and the difference between the control and perturbation experiments are in the right column. The shading denotes the noise levels in FU. Note that cloud ice and snow are present only in FU and FU\*.

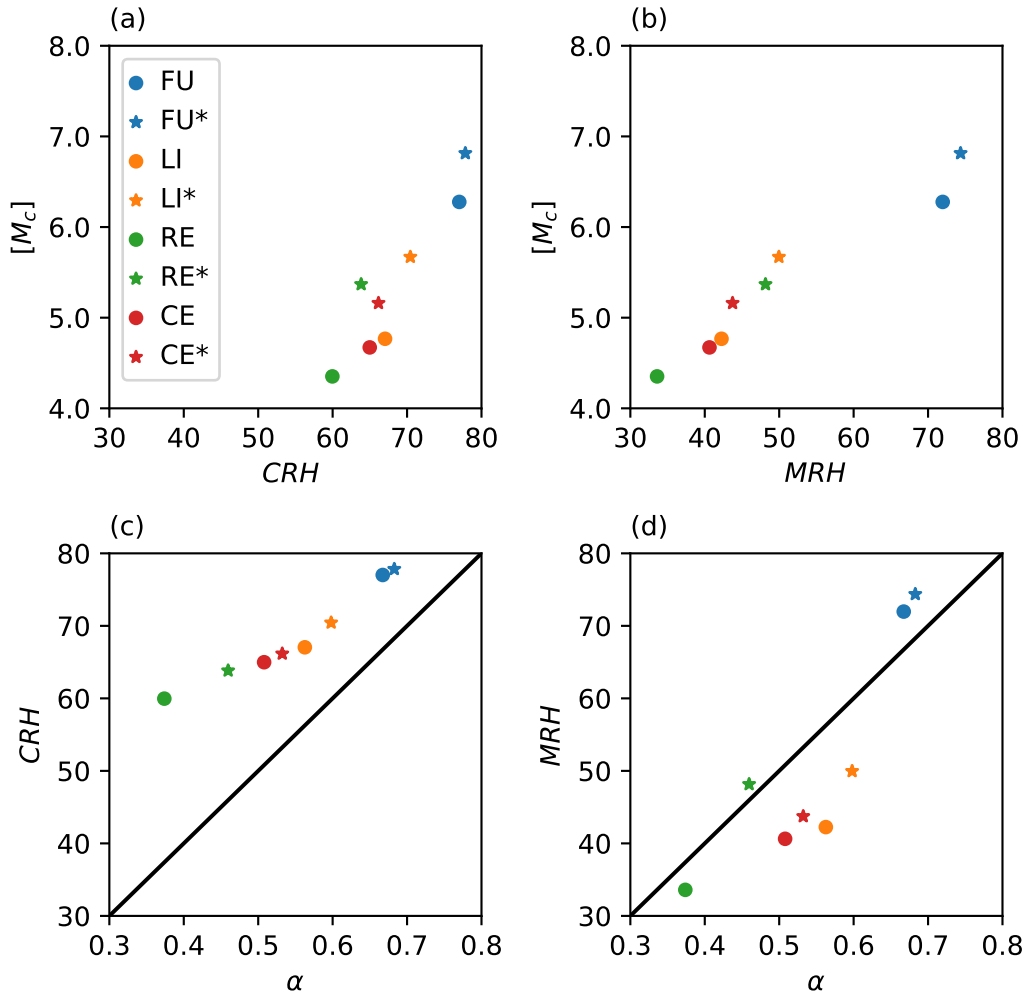
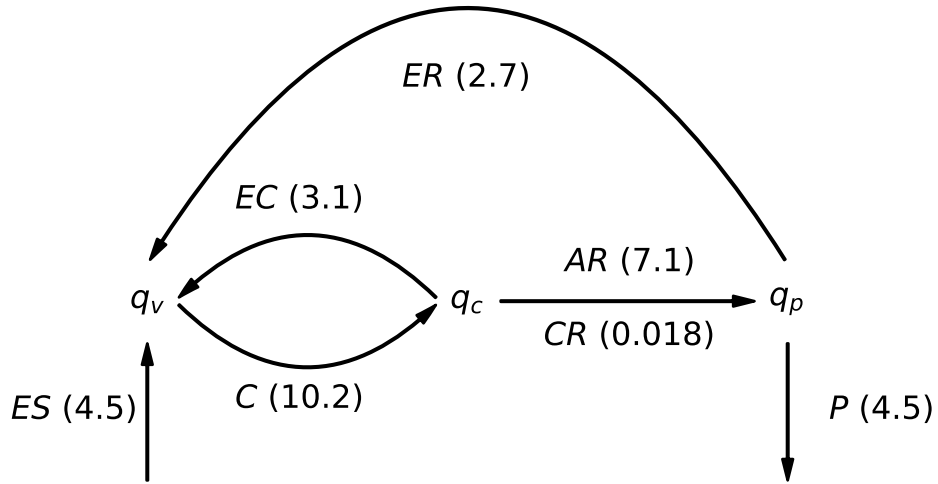


**Figure 2.** Scatter plots of (a) vertically averaged convective mass flux ( $[M_c]$ ,  $\text{g m}^{-2} \text{s}^{-1}$ ) versus column relative humidity ( $CRH$ , %), (b)  $[M_c]$  versus mid-tropospheric (400 to 600 hPa) relative humidity ( $MRH$ , %), (c)  $CRH$  versus the re-evaporation ratio ( $\alpha$ , unitless), and (d)  $MRH$  versus  $\alpha$  in all experiments.

(a)



(b)

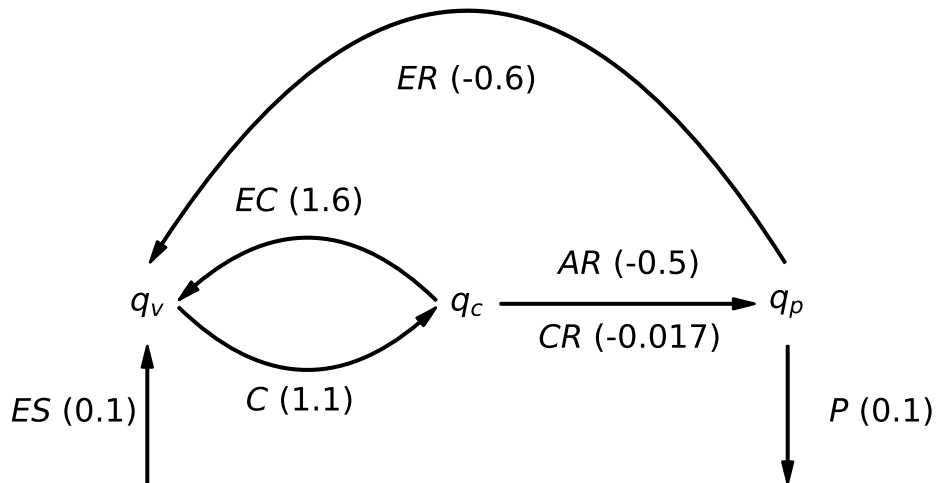


**Figure 3.** Domain-average column-integrated rates (mm day<sup>-1</sup>) of microphysical processes involving water vapor ( $q_v$ ), cloud condensates ( $q_c$ ) and hydrometeors ( $q_p$ ) [condensation of cloud condensates ( $C$ ), re-evaporation of cloud condensates ( $EC$ ), conversion of cloud water to rain by autoconversion ( $CR$ ) and accretion ( $AR$ ) and re-evaporation of rain ( $ER$ )], as well as surface evaporation ( $ES$ ) and precipitation ( $P$ ). (a) is the LI control experiment, and (b) the difference between LI and LI\*. The corresponding values for all configurations are listed in Table 1.

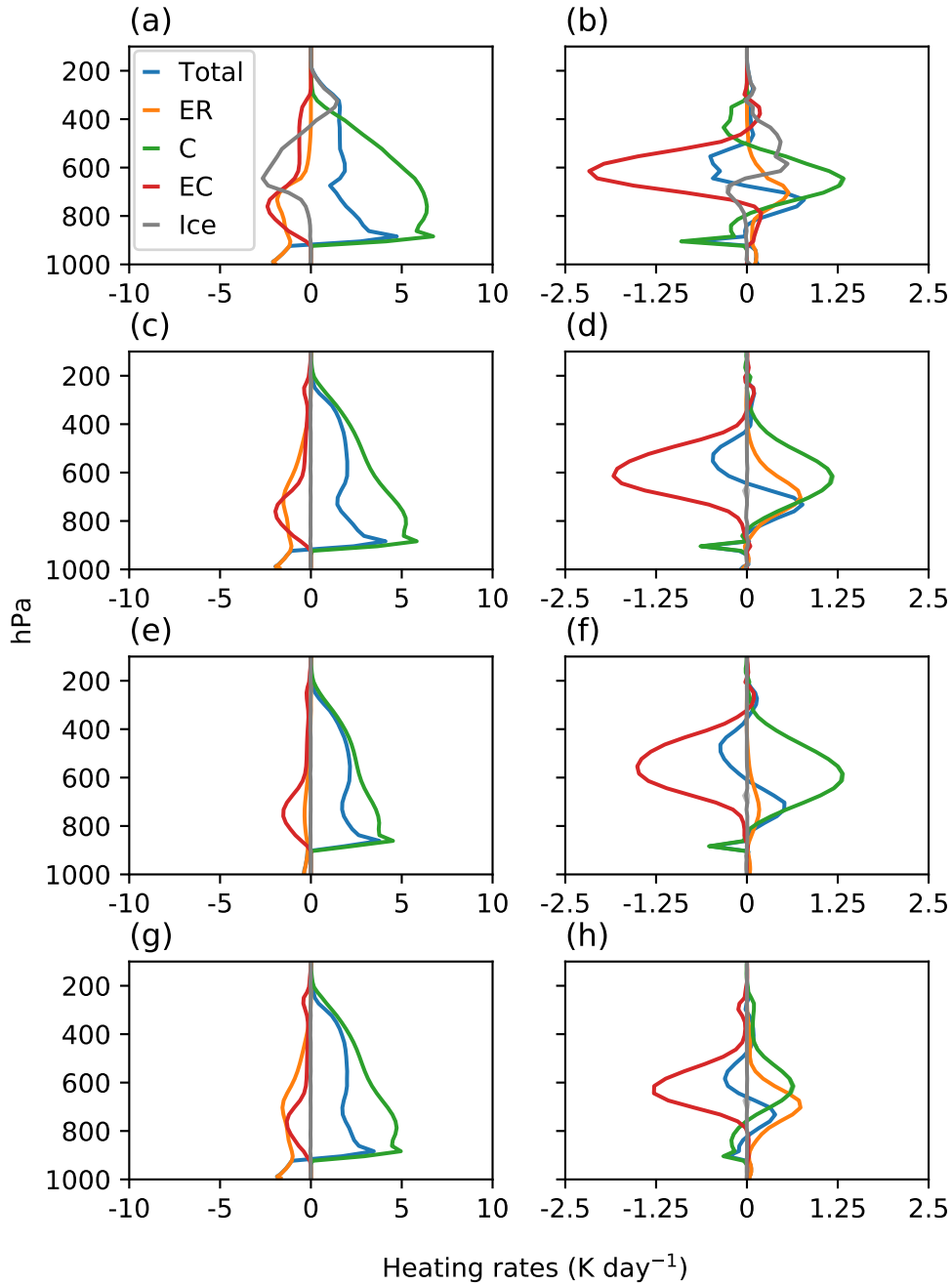


**Figure 4.** Vertical profiles of the domain-average heating rates ( $\text{K day}^{-1}$ ) due to condensation (*C*), rain re-evaporation (*ER*), cloud condensate re-evaporation (*EC*), ice microphysics (*Ice*) and the total (*Total*). The control experiments are in the left column, and the difference between the control and perturbation experiments are in the right column. (a)-(b) are for FU, (c)-(d) for LI, (e)-(f) for RE, and (g)-(h) for CE.